Open access • Proceedings Article • DOI:10.1364/CLEO_AT.2011.JTUI14

Hollow-bottle optical microresonators — Source link

Michalis N. Zervas, Ganapathy Senthil Murugan, Marco N. Petrovich, James S. Wilkinson

Institutions: University of Southampton

Published on: 01 May 2011 - Conference on Lasers and Electro-Optics

Topics: Q factor and Resonator

Hollow-bottle optical microresonators

G. Senthil Murugan,* M. N. Petrovich, Y. Jung, J. S. Wilkinson, and M. N. Zervas

[1]*Optoelectronics Research Centre, University of Southampton, Southampton SO17 1BJ, UK*
**smg@orc.soton.ac.uk*

Abstract: Selective excitation of whispering-gallery and bottle modes in a robust hollow-bottle optical microresonator, fabricated from a silica microcapillary by a pressure-compensated, "soften-and-compress" method, is demonstrated. Characteristic resonance spectra of bottle modes were obtained by using a tapered fiber coupled at different locations along the hollow bottle. The spectral characteristics (Q-factor, excitation efficiency) are shown to have high tolerance to angular misalignment of the tapered fiber. In addition, introduction of localized losses on the outer surface of the resonator results in selective clean-up of the transmission spectrum and superior performance. A theoretical analysis of modal turning points and associated resonant wavelengths is used to explain the mechanism of mode-suppression and the resultant spectral cleaning.

OCIS codes: (140.4780) Optical resonators; (140.3948) Microcavity devices; (230.7408) Wavelength filtering devices; (280.4788) Optical sensing and sensors.

References and links

1. K. J. Vahala, "Optical microcavities," Nature **424**(6950), 839–846 (2003).
2. V. S. Ilchenko and A. B. Matsko, "Optical Resonators with Whispering-Gallery Modes -Part II: Applications," IEEE J. Sel. Top. Quantum Electron. **12**(1), 15–32 (2006).
3. A. B. Matsko and V. S. Ilchenko, "Optical Resonators with Whispering-Gallery Modes -Part I: Basics," IEEE J. Sel. Top. Quantum Electron. **12**(1), 3–14 (2006).
4. M. L. Gorodetsky, A. A. Savchenkov, and V. S. Ilchenko, "Ultimate Q of optical microsphere resonators," Opt. Lett. **21**(7), 453–455 (1996).
5. B. E. Little, J. S. Foresi, G. Steinmeyer, E. R. Thoen, S. T. Chu, H. A. Haus, E. P. Ippen, L. C. Kimerling, and W. Greene, "Ultra-compact Si-SiO2 microring resonator optical channel dropping filters," IEEE Photon. Technol. Lett. **10**(4), 549–551 (1998).
6. D. K. Armani, T. J. Kippenberg, S. M. Spillane, and K. J. Vahala, "Ultra-high-Q toroid microcavity on a chip," Nature **421**(6926), 925–928 (2003).
7. G. Senthil Murugan, Y. Panitchob, E. J. Tull, P. N. Bartlett, D. W. Hewak, M. N. Zervas, and J. S. Wilkinson, "Position-dependent coupling between a channel waveguide and a distorted microsphere resonator," J. Appl. Phys. **107**(5), 053105 (2010).
8. M. Sumetsky, "Whispering-gallery-bottle microcavities: the three-dimensional etalon," Opt. Lett. **29**(1), 8–10 (2004).
9. M. N. Zervas, G. S. Murugan, and J. S. Wilkinson, "Demonstration of novel high-Q fiber WGM "bottle" microresonators", Proc. 10th anniversary International Conference on Transparent Optical Networks **4**, 58 (2008).
10. G. S. Murugan, J. S. Wilkinson, and M. N. Zervas, "Experimental demonstration of a bottle microresonator," in Conference on Lasers and Electro-Optics 2009, OSA Technical Digest Series (Optical Society of America, 2009), paper JTuD87.
11. G. Senthil Murugan, J. S. Wilkinson, and M. N. Zervas, "Selective excitation of whispering gallery modes in a novel bottle microresonator," Opt. Express **17**(14), 11916–11925 (2009).
12. A. A. Savchenkov, A.B. Matsko, D. Strekalov, V.S. Ilchenko and L. Maleki, "Mode filtering in optical whispering gallery resonators," Electron. Lett. **41**, 495 (2005).
13. M. Pöllinger, D. O'Shea, F. Warken, and A. Rauschenbeutel, "Ultrahigh-*Q* Tunable Whispering-Gallery-Mode Microresonator," Phys. Rev. Lett. **103**(5), 053901 (2009).
14. G. S. Murugan, J. S. Wilkinson, and M. N. Zervas, "Optical excitation and probing of whispering gallery modes in bottle microresonators: potential for all-fiber add-drop filters," Opt. Lett. **35**(11), 1893–1895 (2010).
15. Ch. Strelow, H. Rehberg, C. M. Schultz, H. Welsch, Ch. Heyn, D. Heitmann, and T. Kipp, "Optical microcavities formed by semiconductor microtubes using a bottlelike geometry," Phys. Rev. Lett. **101**(12), 127403 (2008).
16. F. Li, Z. Mi, and S. Vicknesh, "Coherent emission from ultrathin-walled spiral InGaAs/GaAs quantum dot microtubes," Opt. Lett. **34**(19), 2915–2917 (2009).
17. M. Sumetsky, Y. Dulashko, and R. S. Windeler, "Optical microbubble resonator," Opt. Lett. **35**(7), 898–900 (2010).

#150530 - $15.00 USD Received 6 Jul 2011; revised 13 Sep 2011; accepted 13 Sep 2011; published 4 Oct 2011

18. H. Li, Y. Guo, Y. Sun, K. Reddy, and X. Fan, "Analysis of single nanoparticle detection by using 3-dimensionally confined optofluidic ring resonators," Opt. Express **18**(24), 25081–25088 (2010).
19. A. Watkins, J. Ward, Y. Wu, and S. Nic Chormaic, "Single-input spherical microbubble resonator," Opt. Lett. **36**(11), 2113–2115 (2011).
20. M. N. Zervas, G. S. Murugan, M. N. Petrovich, and J. S. Wilkinson, "Hollow-Bottle Optical Microresonator", in Conference on Lasers and Electro-Optics 2011, OSA Technical Digest Series (Optical Society of America, 2011), paper JTuI14.
21. I. M. White, H. Oveys, and X. Fan, "Liquid-core optical ring-resonator sensors," Opt. Lett. **31**(9), 1319–1321 (2006).
22. V. Zamora, A. Díez, M. V. Andrés, and B. Gimeno, "Refractometric sensor based on whispering-gallery modes of thin capillarie," Opt. Express **15**(19), 12011–12016 (2007).
23. M. Sumetsky, R. S. Windeler, Y. Dulashko, and X. Fan, "Optical liquid ring resonator sensor," Opt. Express **15**(22), 14376–14381 (2007).
24. X. Fan, I. W. White, H. Zhu, J. D. Suter, and H. Oveys, "Overview of novel integrated optical ring resonator bio/chemical sensors", Proc. SPIE vol. **6452**, 64520M (2007).
25. V. Zamora, A. Díez, M. V. Andrés, and B. Gimeno, "Interrogation of whispering-gallery modes resonances in cylindrical microcavities by backreflection detection," Opt. Lett. **34**(7), 1039–1041 (2009).
26. D. Gloge, "Weakly guiding fibers," Appl. Opt. **10**(10), 2252–2258 (1971).
27. S. Schiller and R. L. Byer, "High-resolution spectroscopy of whispering gallery modes in large dielectric spheres," Opt. Lett. **16**(15), 1138–1140 (1991).
28. C. C. Lam, P. T. Leung, and K. Young, "Explicit asymptotic formulas for the positions, widths, and strengths of resonances in Mie scattering," J. Opt. Soc. Am. B **9**(9), 1585 (1992).
29. Y. Panitchob, G. S. Murugan, M. N. Zervas, P. Horak, S. Berneschi, S. Pelli, G. Nunzi Conti, and J. S. Wilkinson, "Whispering gallery mode spectra of channel waveguide coupled microspheres," Opt. Express **16**(15), 11066–11076 (2008).

1. Introduction

Optical microresonators have proven invaluable both for fundamental research and in a wide range of device applications, such as strong-coupling cavity quantum electrodynamics, efficient microlasers and filters, optical delay lines and miniature sensors [1,2]. They can sustain high-Q resonances based on efficient excitation of whispering gallery modes (WGMs) [1,3] and offer the potential for the implementation of a range of next generation compact, low-power and high speed photonic devices. To date, several different microresonator morphologies, such as microspheres, micro-rings/-discs, and microtoroids, have been studied in depth, each offering its own unique features and advantages [4–6]. Despite their physical differences, efficient operation of these microresonators essentially relies on quasi-2D WGM optical confinement in a single physical plane. In all cases, the optical field extension perpendicular to this plane is much smaller. In the case of perfect microspheres, modes with large polar order exist, which show substantial extension in the perpendicular direction. However, these modes are members of degenerate mode families in which the lowest order mode, confined tightly around the microsphere equator, is in most practical cases preferentially excited. A small microsphere ellipticity is known to break the degeneracy and enables the higher order modes to be individually excited. Even in this case, the orientation of the non-ideal sphere should be controlled in order for the excitation to be strong [7].

Recently, there has been increased activity on a new cylindrical microresonator type, namely the bottle microresonator, which, in contrast with the examples above, shows truly 3-D WGM confinement [8–13]. Bottle microresonators are solid, strong prolate spheroid structures, which support highly non-degenerate WGMs. Depending on the excitation arrangement, a rich variety of modes can be efficiently excited [11], unlike microspheres where mode-degeneracy masks such excitation. Of particular interest are modes that exhibit two well separated spatial regions along the bottle axis with enhanced field strength, corresponding to modal turning points. We have experimentally studied these intensity maxima on both sides of the bottle microresonator near the turning points [9–11] and used them in order to demonstrate add/drop functionality [14].

In addition to solid bottle microresonators, there have been recent demonstrations of hollow (or "empty") bottle microresonators [15,16] formed by semiconductor microtubes, as well as optical microbubble resonators [17–19] formed on optical microcapillaries. In the former configuration, the bottle-like geometry has been achieved by the formation of a parabolic lobe, resulting in an *effective* variation of the axial propagation constant of a rolled-

#150530 - $15.00 USD Received 6 Jul 2011; revised 13 Sep 2011; accepted 13 Sep 2011; published 4 Oct 2011

up microtube. In this case, the effective "bulge" is only a small percentage of the microtube radius and, due to scattering at the inevitable internal and external stepped edges, the resulting Q factors were limited to ~2000-2500. The latter configuration, on the other hand, has been achieved by localised CO_2 laser heating of a pressurised glass microtube. In this case, the microbubble shows a very pronounced "bulge", with its final diameter almost double the original capillary radius.

In this paper, we present a pressure-compensated, "soften-and-compress" method for fabricating high quality hollow micro-bottle resonator (HMBR). We show that the resulting high Q resonances are insensitive to optical excitation angular misalignments, greatly facilitating the optical integration of these devices. We also show that the introduction of a localized scattering loss on the HMBR outer surface preferentially attenuates a subset of the bottle modes and results in substantial spectral "cleaning-up". Finally, mode numbers and the associated resonant wavelengths calculated for experimentally observed resonance spectra of HMBR are used to give physical insight into the spectral cleaning mechanism.

2. Experimental Results

In this paper, we extend our previously published "soften-and-compress" fabrication technique of solid microbottle resonators [9–11] to produce highly-controllable, high performance HMBRs [20]. The HMBRs were fabricated from a glass capillary using a standard fusion splicer. This method has the advantage of being easy to implement, and yet very flexible. First, a glass capillary was fabricated by drawing a high purity synthetic silica tube (Heraeus Suprasil F300) in a fiber drawing tower. The silica tube was first etched on the inside using a standard gas-phase etching procedure and then fire polished on both the inside and outside using a oxy-hydrogen flame. A small positive pressure was applied during fiber drawing in order to maintain the circularity of the capillary cross-section. The outside diameter (OD) of the capillary, D_c, was 218 ± 1μm and the wall thickness, T_c, was approximately 15 ± 1μm. Sections of about 1m length were used for the fabrication of the HMBRs. One end of the capillary was sealed, while the other was connected to a custom-built pressurisation system. In contrast with the technique reported in [17], which relies on high internal pressure only to form the microbubble, our technique relies on a combination of moderate pressure, mainly aimed at counteracting the surface tension in the softened glass, and the "compression" action of the splicer in order to form a highly-controllable-curvature "bottle" shape. The overlap factor of the splicer and pressure within the capillary were optimised independently (our pressurisation system had a resolution of approximately 0.1kPa), which enabled the realization of precise harmonic oscillator profiles [11] in our HMBRs with excellent consistency and reproducibility. At the center of the resonator, the final HMBRs were designed to have ODs, D_b, and wall thicknesses, T_b, of about 265 ± 1μm and 13.5 ± 1μm, respectively. The observed small thinning of the micro-bottle wall is a result of slightly larger internal pressure and overcompensation of the surface tension. The dimensions were determined after the microresonator was sliced carefully at the center and measured using an optical microscope. The control over the resonator curvature is very good and depends on the accuracy of the compression movement of the translation stages of the splicer and the accuracy of the pressurisation. Resonators with thinner walls could be readily obtained by using a capillary fibre with comparatively higher aspect (ID/OD) ratio.

Figure 1 shows a fabricated typical HMBR with dimensions summarised in the caption. The bottle shape was fitted very well with a truncated harmonic-oscillator profile [radius $R(z) = R_b[1+(\Delta k z)^2]^{-1/2}$] with $\Delta k = 0.0027\mu m^{-1}$ [11] (red line). A number of microbottle resonators were fabricated with varying shape curvatures characterized with Δk up to $0.007\mu m^{-1}$. Larger Δk is achievable although the structure starts resembling the micro-bubble resonator [17].

#150530 - $15.00 USD Received 6 Jul 2011; revised 13 Sep 2011; accepted 13 Sep 2011; published 4 Oct 2011

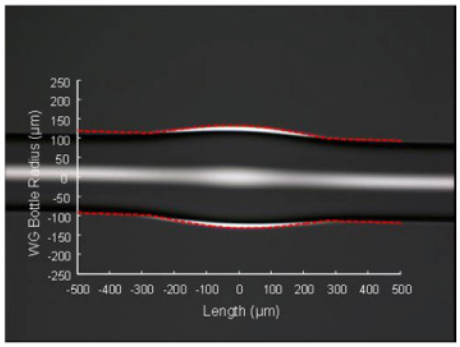

Fig. 1. Hollow-bottle microresonator with fitted truncated harmonic-oscillator profile (red line). Capillary diameter D_c = 218μm, bottle outer diameter D_b = 265 μm, bottle length L_b≈550 μm, wall thickness T_b = 13.5 μm (for the fitted harmonic oscillator profile: $\Delta k = 0.0027\mu m^{-1}$).

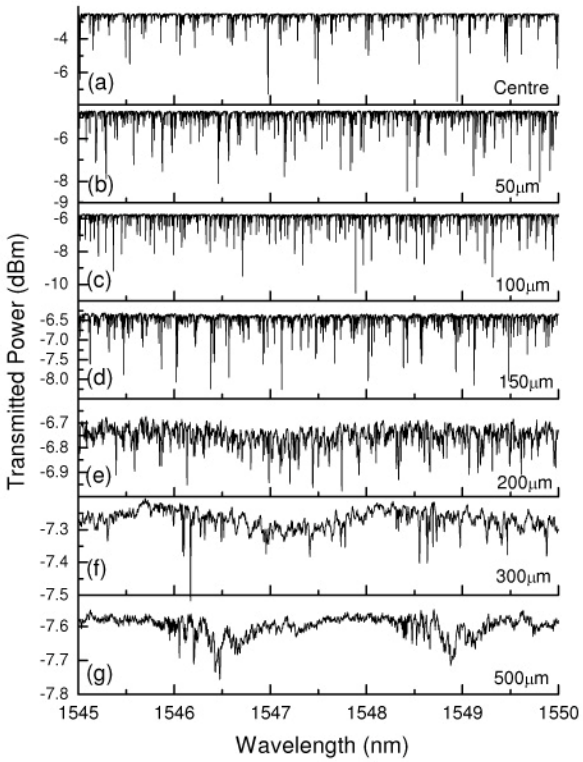

Fig. 2. Transmission spectra of the tapered fiber-coupled hollow-bottle microresonator excited at the center and at several positions along the HMBR. The resonantor length is 550μm.

The modal properties of the HMBR were investigated by optically exciting the resonator via a 2μm diameter tapered fiber. The fiber taper was in physical contact with the microresonator which, while lowering the Q's by loading the resonator, results in extremely stable operation. One of the pigtails of the excitation fiber taper was connected to a tuneable laser (Agilent 81600B, with tuning range from 1440nm to 1640nm and linewidth of 100 kHz) and the output end was connected to an InGaAs detector in order to measure the transmitted light. The fiber taper was coupled to the HMBR at various positions starting from the center of the bottle to the bottle-neck (furthest turning point) and beyond. Transmission spectra collected with the excitation fiber taper at various positions along the bottle are shown in Fig.

#150530 - $15.00 USD Received 6 Jul 2011; revised 13 Sep 2011; accepted 13 Sep 2011; published 4 Oct 2011

2(a-g). Rich and dense spectral characteristics are observed when the excitation tapered fiber is within the bottle section, as shown in Fig. 2(a-e). The highest Q factor of about 10^7 was measured with the tapered fiber at the center. As the excitation fiber is moved towards the bottle neck, both the maximum transmitted power and the Q factor decrease. This behavior is similar to that observed in solid bottle microresonators [11]. When the excitation taper was placed well outside the bottle, only very-low-Q asymmetric resonances were observed. Their free spectral range was 2.41nm at around 1548nm, which corresponds to a cylindrical microresonator with effective OD of 217μm – thus very close to the actual diameter of the capillary. In order to assess the usability of the fabricated HMBRs and their suitability for the implementation of robust, easily integratable devices, we have investigated the dependence of the transmission spectra on the angular alignment of the excitation/collection fiber taper.

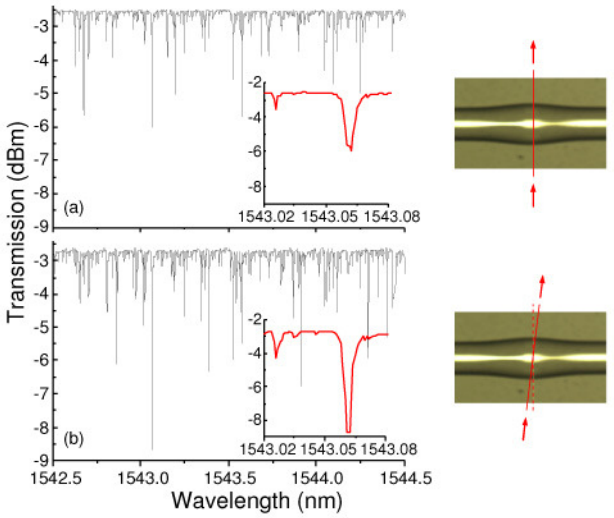

Fig. 3. Transmission spectra of the fiber-coupled hollow-bottle microresonator excited at the center, with the excitation tapered fiber (a) perpendicular to the bottle axis and (b) misaligned by 3.25°.

Figure 3 shows spectra with the HMBR excited at the center, with the excitation fiber taper (a) perpendicular to the bottle axis and (b) misaligned by 3.25°. It can be seen that the wavelengths and Q-factors of the individual resonant dips in the transmission spectrum are essentially insensitive to misalignments of the excitation taper. Actually, as the insets in Fig. 3 show, the magnitudes of some resonances increase and their Q factors improve as a consequence of the small misalignment. This is believed to be due to tilt-induced tuning of the coupling constant rendering it closer to critical coupling. High-Q resonances, albeit with lower excitation efficiency, were observed even at extreme tilt angles of 45°. The full investigation and theoretical analysis of this effect is beyond the scope of this paper. The relaxed requirements on excitation-fiber alignment are in sharp contrast with those for standard hollow cylindrical microresonators, such as micro-capillaries, used in various optofluidic sensor applications [21–23]. In the case of these cylindrical microresonators inevitable spreading of the launched light results in spiral modes and asymmetrically broadened spectra, so that very precise alignment [24] and/or monitoring of backscattered light [25] are needed to minimise spreading and maximise the resonance Q. In the HMBR case, the diverging light is reflected back at the corresponding turning points, resulting in high-Q resonances being maintained.

The dense spectral features shown in Fig. 2 are highly advantageous when bottle microresonators are used in cavity QED studies [13]. However, such spectral characteristics may be a serious hindrance if HMBRs were to be used as refractometric optofluidic sensors. In this case, a “cleaner” spectrum with more easily identifiable and traceable spectral features

#150530 - $15.00 USD Received 6 Jul 2011; revised 13 Sep 2011; accepted 13 Sep 2011; published 4 Oct 2011

would be desirable. As discussed before [11], the rich spectral features are a result of the strongly broken degeneracy between whispering gallery modes with common azimuthal and differing axial mode numbers, as a result of the highly prolate shape. In addition to different Eigen frequencies, these non-degenerate resonances exhibit substantially different spatial intensity distributions along the bottle length [11]. This property of the resonant modes in a bottle resonator can be exploited to differentially attenuate some of the modes according to axial mode-number and thereby substantially "clean up" the spectrum.

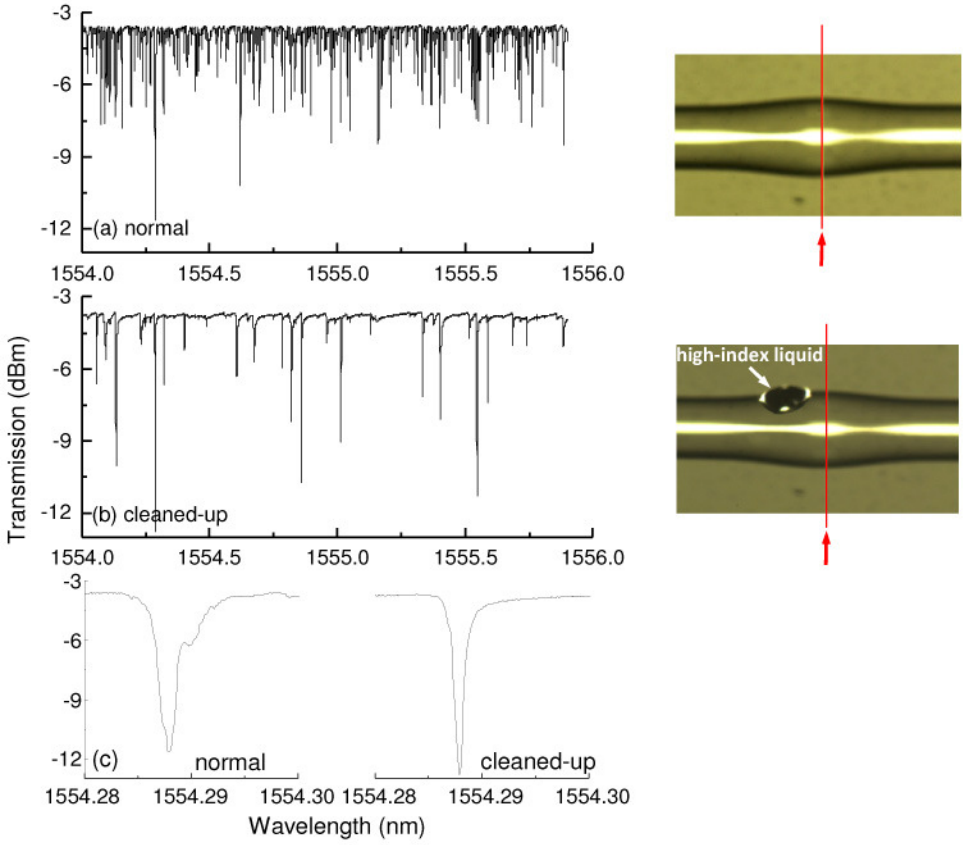

Fig. 4. (a) Normal transmission spectrum of the fiber-coupled hollow-bottle microresonator excited at the center, and (b) cleaned-up spectrum with localized loss element placed on the bottle outer surface, (c) detailed comparison of an individual resonance before and after "cleaning-up". Cleaning-up liquid refractive index = 1.64.

Figure 4(a) shows the normal spectrum of the HMBR excited at the center. Figure 4(b), on the other hand, shows the "cleaned-up" spectrum, with a loss element placed away from the center near the bottle edge (as shown in the inset). In this case the loss was introduced by applying a small drop of index matching liquid (Cargille) of refractive index 1.64 in different positions along the bottle length. This is similar to the modal filtering method applied to cm-sized crystalline disks using an auxiliary out-coupling prism [12]. However, our method is suitable for micrometer-scale resonators. The clean spectrum consists of modes that occupy the central part of the bottle and therefore do not suffer the extra loss and resultant deterioration in Q due to the loss element. Figure 4(c) shows a narrow wavelength range in the transmission spectrum where it can be seen that even a single spectral feature originally consists of a superposition of several modes, and that these are reduced to predominantly one when the loss element is added. In addition, the surviving resonance in this case becomes slightly stronger. This behavior is discussed further below. The localized loss could be

#150530 - $15.00 USD Received 6 Jul 2011; revised 13 Sep 2011; accepted 13 Sep 2011; published 4 Oct 2011

introduced in a number of different ways, such as controlled deposition of lossy layers, partial recoating with high-index polymer material and partial surface roughening.

From the data in Fig. 3 and Fig. 4 we observe that in addition to robustness against misalignment and the spectral "cleaning", most of the transmission resonances increase in magnitude. In the case of misalignment, wavefront tilt is believed to decrease the overall coupling constant (integrated along the length of the coupled region) of an initially overcoupled system, resulting in coupling closer to the critical value. In the case of the "cleaned-up" spectrum, the extra scattering losses are believed to reduce the Q and bring the system closer to critical coupling.

3. Bottle Microresonator Mode Theory

3.1 Modal characteristics

Bottle microresonator modes of a given polarization are characterized by three modal numbers (m,p,q), where $2m$ (m = 0,1,2,…) gives the number of field nodes around the circumference, p (p = 1,2,…) gives the number of power maxima along the radius, and q (q = 0,1,2,…) gives the number of field nodes along the axis of the microresonator. In the scalar approximation, the transverse electric field is given by $E(\mathrm{r},\varphi,\mathrm{z}) = \Phi(\mathrm{r},\mathrm{z})\Psi(\mathrm{z})\exp(\mathrm{i}m\varphi)$ [8,13], where the radial distribution of the field is given by [26]:

$$\Phi(r,z)=\begin{cases} A_m \dfrac{J_m\left(U_{mp}\, r/R(z)\right)}{J_m(U_{mp})} & r \le R(z) \\ A_m \dfrac{K_m\left(U_{mp}\, r/R(z)\right)}{K_m(U_{mp})} & r > R(z) \end{cases} \tag{1}$$

In highly multimoded fibers, ignoring polarization effects U_{mp} is approximated by the p^{th} root of the $J_{\mathrm{m}}(U)$ function. U_{mp} can also be approximated by the analytical expression [27,28]:

$$U_{mp} = m + \alpha_p \left(m/2\right)^{1/3} + \left(3/20\right)\alpha_p^2 \left(m/2\right)^{-1/3} \tag{2}$$

where α_{p} is the p^{th} root of the Airy function (α_{p} = 2.3381, 4.0879, 5.5205, 6.7867, 7.9441 for p = 1,2,3,4,5 respectively). The two aforementioned approximations give almost identical results. In the case of a harmonic oscillator profile, the axial distribution of the field is given analytically by:

$$\Psi(z) = C_{mq} H_q\left(\sqrt{\frac{\Delta E_m}{2}}\, z\right)\exp\left(-\frac{\Delta E_m}{4} z^2\right) \tag{3}$$

where $\Delta E_{\mathrm{m}} = 2U_{\mathrm{mp}}\Delta k/R_{\mathrm{b}}$, H_{q} is the m^{th} order Hermite polynomial and $C_{\mathrm{mq}} = [\Delta E_{\mathrm{m}}/(\pi 2^{2q+1}(q!)^2)]^{1/4}$. The axial spreading of each mode is defined by the corresponding turning point, given by [11]:

$$z_c = \pm\left[\frac{4}{\Delta E_m}\left(q+\frac{1}{2}\right)\right]^{1/2} \tag{4}$$

measured from the bottle center. Beyond this point the mode is evanescent. The resonant wavelength for each (m,p,q) mode is given by:

$$\lambda_{mpq} = 2\pi n_0\left[\left(\frac{U_{mp}}{R_b}\right)^2 + \left(q+\frac{1}{2}\right)\Delta E_m\right]^{-1/2} \tag{5}$$

#150530 - $15.00 USD Received 6 Jul 2011; revised 13 Sep 2011; accepted 13 Sep 2011; published 4 Oct 2011

When Δk=0 [R(z) = R_b: the case of a cylindrical resonator], Eq. (5) reduces to the well-known formula $\lambda_{mp}=2\pi n_0 R_b/U_{mp}$ giving the resonant wavelength of the (m,p) mode supported by a cylindrical resonator of radius R_b. In all calculations, we have used the experimentally obtained values shown in the caption of Fig. 1.

Based on our calculations, when compared to the excitation fiber, microbottle modes with p>3 exhibit highly mismatched propagation constants and are not expected to show significant excitation. Figure 5(a) shows details of the intensity distribution for mode (733,3,4) along the microbottle length. Figure 5(b), on the other hand, shows the intensity distribution of the same mode over the transverse cross-section of the microbottle. The resonant wavelength is 1554.61nm and the corresponding turning point is 24.8μm. For the modes with $p\leq3$ considered in this study, the radial extent of the field radial is much smaller than the wall thickness and, therefore, the effect of the inner glass/air interface can be ignored. The field penetration of the mode shown in Fig. 5 is about 6μm. The penetration for p=1 and 2 modes is even smaller. The small penetration of these modes justifies the use of Eqs. (1) that strictly apply to solid microbottle resonators. Higher radial-order modes and/or thinner wall thicknesses would require a modification of Eqs. (1) to take into account the inner glass/air interface. Note that in Fig. 5(a) dimensions are truncated in order to emphasize some of the intensity distribution characteristics.

For the microbottle resonator dimensions realized here, for a fixed q and consecutive azimuthal mode numbers m around 755, the calculated wavelength spacing is about 2.1nm. This value increases to about 2.3nm for m varying around 720. On the other hand, for fixed m and consecutive axial mode numbers q, the wavelength spacing is about 0.7nm. As a result the various mode orders are strongly interleaved and result in transmission spectra with extremely complex characteristics, as demonstrated experimentally in Fig. 2, Fig. 3 and Fig. 4(a).

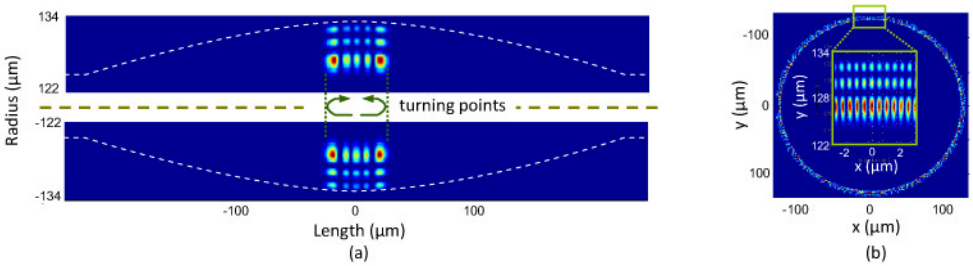

Fig. 5. Intensity distribution (a) along the length and (b) over transverse cross-section of the microbottle for mode (733,3,4). The resonant wavelength and turning point are 1554.61nm and 24.8μm, respectively.

3.2 Modal filtering, mode resonant wavelengths and corresponding turning points

Modal filtering by preferential attenuation, as used in this work, restricts the maximum attainable axial mode number and thereby greatly reduces the number of resonances measured in the transmission spectrum. More specifically, only those modes with turning points before the position of the high-index liquid drop have their loss substantially unaffected and therefore show strong excitation (see Fig. 6(a)). The remainder of the HMBR modes experience very strong scattering losses and are effectively suppressed (see Fig. 6(b)). The scattering loss has not actually been modeled and, therefore, the relative power intensities of Fig. 6(a) and (b) do not reflect the effect of this loss.

#150530 - $15.00 USD Received 6 Jul 2011; revised 13 Sep 2011; accepted 13 Sep 2011; published 4 Oct 2011

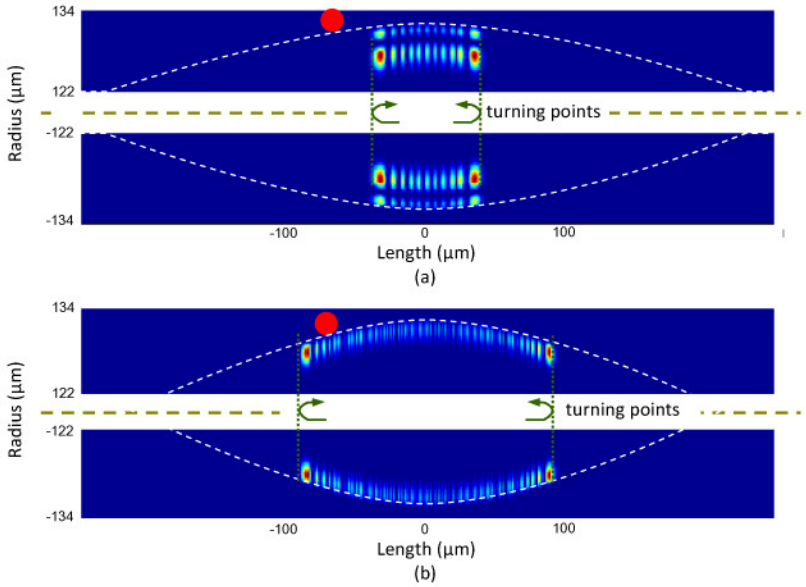

Fig. 6. Power distribution of: (a) an un-attenuated mode (742,2,10) with resonant wavelength 1554.13nm and turning point 36μm, and (b) a mode (738,1,58), which would experience a strong diffractive loss from a high-index liquid drop placed at the position of the red dot (resonant wavelength is 1555.65nm and turning point is 90.5μm).

Figure 7(a) shows the azimuthal mode number m and the corresponding turning point for the various microbottle modes for modes with radial mode number p = 1(○), 2(+) and 3(Δ). The corresponding axial mode numbers are q = 0,1,2,3,… and for each radial mode family (fixed p) they increase from left to right. The maximum q number shown in the Figure in this case is 29, which corresponds to a turning point of about 65μm. Inclusion only of modes with turning points at less than 65μm models closely the experimental case where modes are suppressed by the drop of high-index liquid. The 65μm chosen is slightly shorter than the actual position of the drop which, as the inset of Fig. 4(b) indicates, is at about 70μm from the center. This is to accommodate the evanescent field extent of the surviving modes, which is typically about 5μm. The modes are selected so that their resonant wavelengths lie in the range 1554nm to 1556nm as shown in Fig. 7(b). The resonant wavelengths are calculated using Eq. (5). It is shown that within this spectral range, for each radial order, the modes are organized in three sub-groups separated by ~0.7nm. As mentioned earlier, modes in the three sub-groups with the same radial number correspond to the same azimuthal numbers and consecutive axial numbers. Within each sub-group adjacent modes are characterized by consecutive azimuthal mode numbers and q, q + 3 axial mode numbers. The modal spacing within each sub-group increases as the q number increases. The average modal spacing in the sub-groups with radial mode number p = 1, 2 and 3 is about 0.03nm, 0.04nm and 0.05nm respectively. This feature can be used to aid the mode identification in the next sub-section.

#150530 - $15.00 USD Received 6 Jul 2011; revised 13 Sep 2011; accepted 13 Sep 2011; published 4 Oct 2011

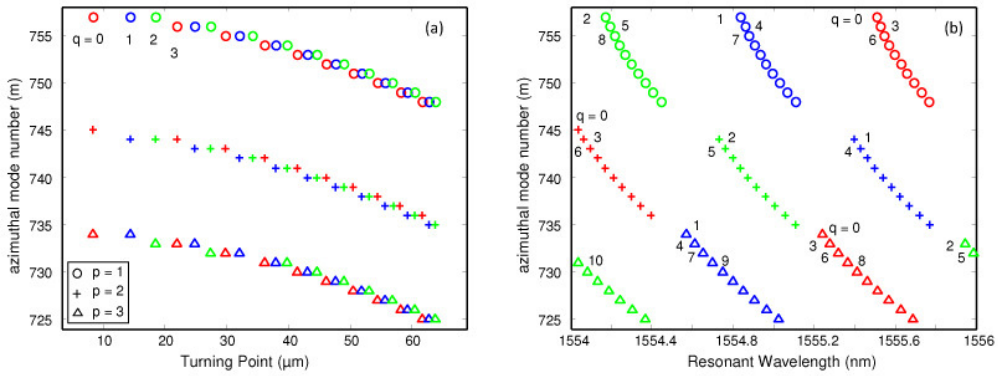

Fig. 7. (a) Azimuthal mode number versus turning point and (b) azimuthal mode number versus resonant wavelength.

In the absence of any modal filtering mechanisms, all the modes are potentially excited. Figure 8(a) shows the azimuthal mode number m and the corresponding turning point for the microbottle modes for p = 1(○), 2(+) and 3(Δ). The corresponding axial mode numbers are q = 0,1,2,… and again increase from left to right. The q number shown in this figure is limited to 279. This corresponds to a turning point of ~155μm. The resonator supports modes with higher axial mode numbers and longer turning points, which are not included for clarity. Figure 8(b) shows the associated resonant wavelengths. It is shown that the modes of different order interleave in a complex manner and result in very dense spectral characteristics. This is reflected in the experimental transmission spectra for the bottle resonator with no added high-index drop as a mode filter (see Fig. 2, Fig. 3 and Fig. 4(a)).

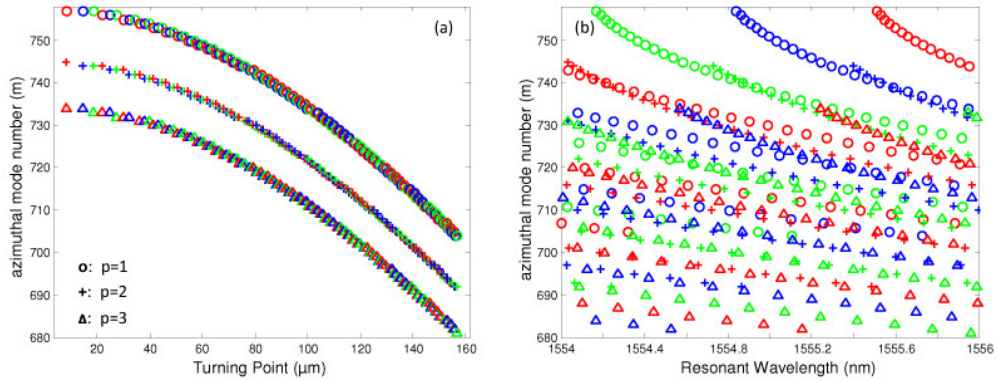

Fig. 8. (a) Azimuthal mode number versus turning point and (b) azimuthal mode number versus resonant wavelengths for longer turning point range.

3.3 Comparison with experimental data

The theoretical results of the previous sub-section are used to further understand the main spectral features of the "cleaned-up" and normal experimental data. Figure 9 superimposes the "cleaned-up" experimental data of Fig. 4(b) and the results of Fig. 7(b). The experimental data can be broadly categorized into three different groups. Within the spectral range shown, groups A and B show three sub-groups while group C shows only two sub-groups. The theoretically predicted resonant wavelengths overlap strongly over three different spectral ranges which align well with the composite groups (B1, A1), (C1, B2, A2) and (C2, B3, A3).

#150530 - $15.00 USD Received 6 Jul 2011; revised 13 Sep 2011; accepted 13 Sep 2011; published 4 Oct 2011

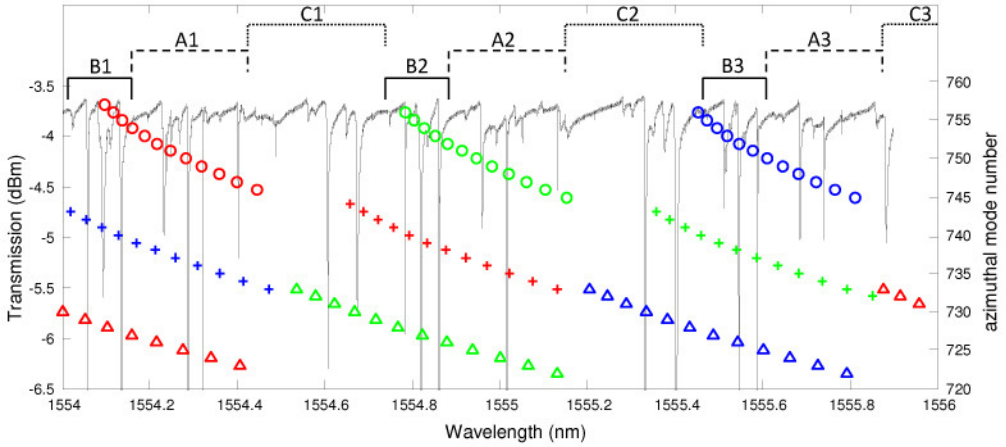

Fig. 9. Experimental "cleaned-up" spectrum. Superimposed are the theoretical resonant wavelengths and the corresponding azimuthal mode numbers (right axis). The corresponding radial mode numbers are p = 1(○), 2(+) and 3(Δ).

Under closer inspection, group B appears to align well with modes characterized by p = 2. The experimental wavelength spacing within this group is ~0.04nm which agrees very well with the theoretical average discussed previously. Group A, on the other hand, appears to align predominantly with the p = 1 modes. It shows main resonances with average spacing of ~0.025nm, which agrees reasonably well with the corresponding theoretical average spacing of ~0.03nm. Finally, Group C appears to align predominantly with the p = 3 modes. It shows main resonances with average spacing of ~0.06nm, which again agrees reasonably well with the corresponding theoretical average spacing of ~0.05nm. In addition, Group C shows minor resonances with spacing of ~0.025nm, most likely as a result of the Group A spectral overlap.

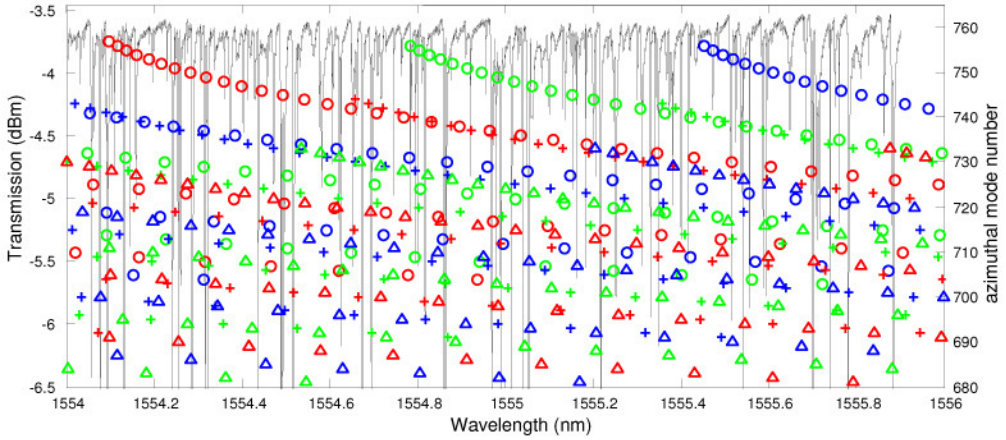

Fig. 10. Experimental normal spectrum. Superimposed are the theoretical resonant wavelengths and the corresponding azimuthal mode numbers (right axis).

In the case of the normal spectrum, shown in Fig. 10, it is obvious that the much denser experimental spectral resonances reflect the presence of a large number of strongly overlapping and interleaved modes of different orders. The excitation strength of each mode will depend on the coupling coefficient between the fundamental mode of the microtaper and each individual microbottle mode as well as the round-trip losses of that mode, in common with microsphere resonators [29]. The coupling constant in turn is a function of the evanescent field overlap and the mismatch in propagation coefficient mismatch the modes under consideration.

#150530 - $15.00 USD Received 6 Jul 2011; revised 13 Sep 2011; accepted 13 Sep 2011; published 4 Oct 2011

Although the theoretical results agree well with the cleaned-up experimental data in Fig. 9, no attempt was made to accurately fit the full population of resonances in Fig. 10. The resonance wavelengths of high axial-number modes included in Fig. 10 depend much more sensitively on the exact shape of the microbottle (as described by Δk), especially close to the bottle necks. In addition, a number of these theoretically predicted modes are not excited significantly because of poor overlap with the microfiber mode. The detailed modal excitation behavior is part of an ongoing study.

4. Summary

In summary, we have presented a pressure-compensated, "soften-and-compress" method for fabricating high quality hollow-bottle optical microresonators. This new class of glass microresonator exhibits rich optical spectra, which depend on the excitation position, similar to their solid counterparts [11]. For central excitation they also show very high Q factors ($\sim 10^7$). In addition, wavelengths and Q factors of the modes observed in the fiber-taper-coupled transmission spectrum show improved insensitivity to optical excitation misalignments, when compared with cylindrical resonators, greatly facilitating the interrogation and optical integration of these devices. We have also shown that the introduction of a localized scattering loss on the outer surface of the HMBR preferentially attenuates bottle modes with turning points further from the bottle center and results in substantial "clean-up" of the WGM spectrum. This is expected to improve the performance of these devices substantially when used as tunable filters or refractometric and optofluidic sensors. Finally, the controlled curvature and smooth bottle shape will facilitate laminar flow in potential optofluidic applications.

Finally, mode numbers and the associated resonant wavelengths of the experimental HMBR have been calculated and used to give physical insight into the spectral cleaning mechanism, showing very good agreement with the experiment.

#150530 - $15.00 USD Received 6 Jul 2011; revised 13 Sep 2011; accepted 13 Sep 2011; published 4 Oct 2011